

Autophagy core protein BECN1 is vital for spermatogenesis and male fertility in mice[†]

Lu Ke¹, Xinyi Lin¹, Yuchuan Luo¹, Siming Tao¹, Chang Yan¹, Yifeilong He¹, Yingjie Wu¹, Ning Liu^{1,2} and Yinghe Qin^{1,*}

- ¹State Key Laboratory of Animal Nutrition and Feeding, College of Animal Science and Technology, China Agricultural University, Beijing, China
- ²Beijing Advanced Innovation Center for Food Nutrition and Human Health, China Agricultural University, Beijing, China
- *Correspondence: State Key Laboratory of Animal Nutrition and Feeding, College of Animal Science and Technology, China Agricultural University, 2 Yuanmingyuan West Road, Haidian, Beijing 100193, China. Tel: +861062731022; Fax: +861062731022; E-mail: qinyinghe@cau.edu.cn

Abstract

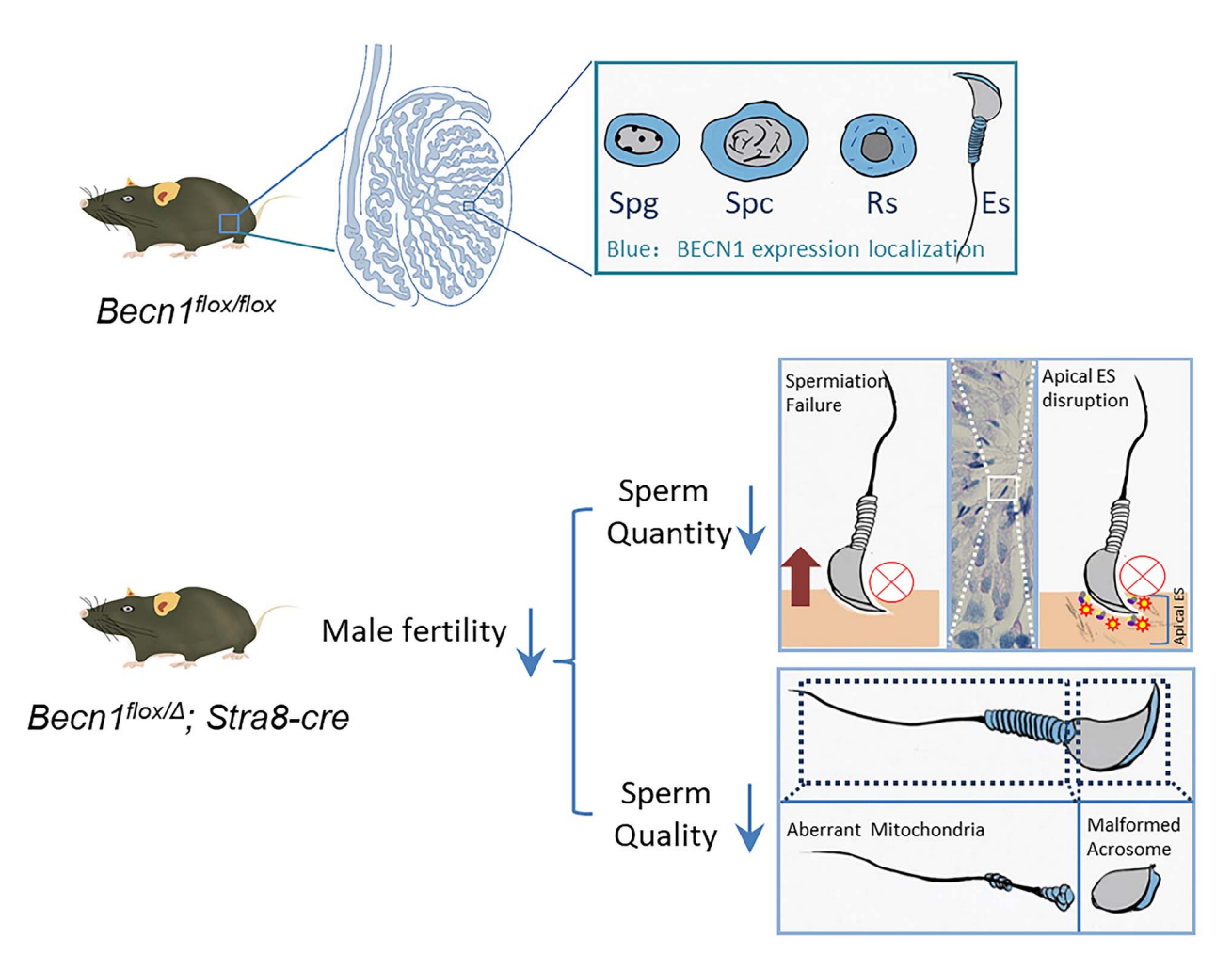
Mammalian spermatogenesis is a highly complex multi-step biological process, and autophagy has been demonstrated to be involved in the process of spermatogenesis. Beclin-1/BECN1, a core autophagy factor, plays a critical role in many biological processes and diseases. However, its function in spermatogenesis remains largely unclear. In the present study, germ cell–specific Beclin 1 (*Becn1*) knockout mice were generated and were conducted to determine the role of *Becn1* in spermatogenesis and fertility of mice. Results indicate that *Becn1* deficiency leads to reduced sperm motility and quantity, partial failure of spermiation, actin network disruption, excessive residual cytoplasm, acrosome malformation, and aberrant mitochondrial accumulation of sperm, ultimately resulting in reduced fertility in male mice. Furthermore, inhibition of autophagy was observed in the testes of germ cell–specific *Becn1* knockout mice, which may contribute to impaired spermiogenesis and reduced fertility. Collectively, our results reveal that *Becn1* is essential for fertility and spermiogenesis in mice.

Summary Sentence Autophagy core protein BECN1 is required for male fertility and spermiogenesis through maintaining normal autophagy function in germ cells.

[†] Grant Support: The work was supported by the National Key Research and Development Program of China (2023YFD1302005) Earmarked Fund for Modern Agro-Industry Technology Research System (CARS-43), National Natural Science Foundation of China (No. 32000082), Major Research Development Program of Xinjiang Uygur Autonomous Region (2020B01004), and Major Scientific and Technological Projects for the Breeding of New Agricultural Varieties in Zhejiang Province (2021c02068-7).

Graphical Abstract

BECN1 is essential for fertility and spermiogenesis in mice



Key words: acrosome, autophagy, BECN1, mitochondria, spermiogenesis

Introduction

Mammalian spermatogenesis is a highly specialized process of cell differentiation in which spermatogonial stem cells (SSCs) in the testis are transformed into haploid sperm via mitosis and meiosis [1]. During spermiogenesis, germ cells undergo enormous structural changes, including the generation of the acrosome, condensation of nuclear chromatin, rearrangement of mitochondria, assembly of sperm flagella, and removal of unnecessary cytoplasm to produce functional sperm, which requires a balance between degradation and energy supply to maintain cellular and metabolic homeostasis [2, 3]. Autophagy is a conserved intracellular process, and three primary types autophagy have been described: macroautophagy (hereafter referred to as autophagy), microautophagy, and chaperone-mediated autophagy [4]. Autophagy is responsible for the degradation of unnecessary cytoplasmic or dysfunctional components through formation of autolysosome resulting from the fusion between outer membrane of the autophagosome with lysosomes [5]. More than 40 autophagy-related (ATG) proteins have been

characterized in autophagy [6]. The initiation is sustained by activation of ATG1/UN51-like Ser/Thr kinases1 (ULK1) complex, and then the nucleation stage depends on Vps34-BECN1 complex to form phagophore. After the formation of pre-autophagosomal structure, the phagophore will continue to extend. This process is mediated by two ubiquitin-like coupling systems, one of which ubiquitin-activating E1-like enzyme, ATG7, activates ATG12 and then facilitates ATG12-ATG5-ATG16L1 complex formation. The complex has an E3-like ligase activity that promotes the transfer of LC3 from ATG3 to the substrate phosphatidylethanolamine (PE) by activating the ATG3 enzyme, forms lipid-soluble LC3-PE, and participates in autophagosome extension. Finally, the fusion of autophagosome and lysosome was completed [7]. In mammals, autophagy functions in cell growth, anti-aging, cellular homeostasis, and cell differentiation [8]. Growing evidence demonstrate that autophagy is involved in processes associated with germ cell development, such as the key pathophysiological processes in many diseases of the male reproductive system [9], survival of testicular cells [10], and

spermatogenesis [3], to ensure male reproductive function. Recently, the molecular mechanism by which autophagy regulates spermatogenesis has been revealed [11–13].

The class III phosphatidylinositol 3-kinase (Ptdlns3K) complex is an autophagy-inducing complex that regulates the autophagosome biogenesis [14]. Phosphipdylinositol-3-phosphate (PtdIns3P) is the product of PtdIns3K that has been reported to be involved in the formation of autophagosomal membranes, and to promote the recruitment of other ATG proteins to promote autophagy [15]. The mammalian autophagy gene Becn1, an ortholog of the Atg6 gene in yeast, is a key component of Ptdlns3K, which serves as the platform for complex assembly and stimulates complex activity [16, 17]. The function of BECN1 is to maintain the localization of other autophagy proteins to phagophore assembly site [18]. Notably, Becn1 null mice show more severe embryonic phenotype than other autophagy gene-deficient mice, which die in early embryonic day 7.5 or earlier [19]. In females, conditional knockout of Becn1 in mouse granulosa cells results in premature delivery and abortion in pregnant mice [20]. In males, BECN1 is localized to the acrosome of round spermatids, suggesting a key role in spermiogenesis [13]. Furthermore, knockdown of Becn1 in TM3 mouse Leydig cells results in decreased testosterone production [21]. However, the regulatory mechanism of BECN1 in male spermatogenesis remains largely unclear.

To investigate the role of BECN1 in the regulation of spermatogenesis, germ cell–specific *Becn1* conditional knockout mice were generated in the present study. Interestingly, we found that *Becn1*-mutant male mice presented reduced fertility, decreased sperm motility and quantity, excessive residual cytoplasm, acrosome malformation, aberrant mitochondrial accumulation, disrupted actin network disruption, and partial failure of spermiation. Thus, our findings reveal that *Becn1* is necessary for normal spermiogenesis and fertility through maintaining autophagy flux in mice.

Materials and methods

Animals

All the animal experimental procedures were approved by the Institutional Animal Care and Use Committee of China Agricultural University. Becn1flox/flox mice were generated by ES cell targeting based on homologous recombination (Shanghai Model Organisms, Shanghai, China). Becn1flox/d; Stra8-cre mice were generated from the cross of Becn1flox/flox mice and Stra8-cre mice (Jackson Laboratory, 008208). Becn1flox/flox mice and Stra8-cre mice are on C57BL/6J genetic background. Wild-type (WT) C57BL/6J mice were purchased from SPF Biotechnology Co., Ltd. (Beijing, China). Genomic DNA was extracted from mouse tails using the Blood/Tissue/Cell Genome Extraction Kit (TIANGEN, DP304-03). Primers used for the genotyping are listed in Supplementary Table S1.

Chemicals and reagents

The following antibodies and reagents were used: rabbit anti-BECN1 (Proteintech Group, 11306-1-AP), mouse anti-PLZF (Santa Cruz Biotechnology, sc-28319), mouse anti-ACRV1 (Santa Cruz Biotechnology, sc-398536), rabbit anti-ACRV1 (Proteintech Group, 14040-1-AP), mouse anti-ADAM3 (Santa Cruz Biotechnology, sc-365288), rabbit

anti-LC3A/B (Cell Signaling Technology, 12741), rabbit anti-ATG5 (Cell Signaling Technology, 12994), rabbit anti-MVH (Abcam, ab13840), rabbit anti-HADHA (Abcam, ab203114), rabbit anti-p62 (Cell Signaling Technology, 5114), FITC-phalloidin (Yeason, 40735ES75), mouse anti-γH2AX-Alexa Fluor 488 (Thermo Fisher Scientific, 05-636), Alexa Fluor 488-conjugated goat anti-rabbit IgG (Abcam, ab150081), Alexa Fluor 555-conjugated goat anti-mouse IgG (Abcam, ab150118), mouse anti-β-actin-horseradish peroxidase (HRP) (Abcam, ab49900), and TUNEL cell apoptosis detection kit (Beyotime Biotechnology, C1089).

Spermatogenic cell smear

The method used here was slightly modified as previously described [22]. Seminiferous tubules were obtained by removing the tunica albuginea of the mouse testis and then were placed in 5 mL of Dulbecco modified Eagle medium (Thermo Fisher Scientific, 11965092) containing 1 mg/mL DNase I (Sigma-Aldrich, EN0521) and 0.5 mg/mL collagenase IV (Sigma-Aldrich, C5138) with gentle mixture. The spermatogenic cell suspension was digested in a water bath set at 32°C for 30 min, and it was removed and mixed upside down every 8 min. The supernatant was discarded after centrifugation, and the cells were resuspended with 5 mL of phosphate-buffered saline (PBS) and centrifuged as indicated above. The supernatant was discarded, and the cells were fixed with 5 mL of 4% PFA by gentle shaking for 15 min at room temperature. The supernatant was discarded after centrifugation, and the cells were resuspended with 5 mL of PBS solution and centrifuged as above indicated. The washing steps were repeated for three times. Finally, the supernatant was discarded, and the cells were resuspended with a minimal volume of PBS, evenly spread on microscope slides (Citotest, 188105W), and dried at room temperature.

Real-time quantitative polymerase chain reaction

RNA was extracted and reverse-transcribed as previously described [23]. In brief, total RNA was extracted from testis using the TRIzol reagent (Sigma-Aldrich, T9424). Complementary DNA was synthesized using the FastQuant RT kit (TIANGEN, KR116-02). Real-time quantitative polymerase chain reaction was performed using the SYBR SuperReal Kit (TIANGEN, FP205-02) on a CFX96 qPCR Detection System (Bio-Rad, California, USA). Primers used for the qPCR analyses are listed in Supplementary Table S2.

Fertility testing

For the fertility test, 2–4-month-old *Becn1*^{flox/ Δ}; *Stra8-cre* and *Becn1*^{flox/flox} male sexually mature mice were paired with two random adult female mice (WT C57BL/6J mice) for at least 2 months. The number of offspring from each pregnancy was recorded.

Histological analysis

Testes and cauda epididymides were fixed with 4% paraformaldehyde (PFA) overnight at 4°C, dehydrated, and embedded in paraffin. Sections of 5 μ m thickness were generated and mounted on glass slides. After deparaffinization, the sections were stained with hematoxylin and eosin (Beyotime Biotechnology, C0105M) or PAS (Beijing Cool Laibo Technology co., ltd, SL7640) according to the manufacturers' instructions.

Epididymal sperm counts, motility, and morphology

Cauda epididymides were dissected from 2-month-old $Becn1^{flox/\Delta}$; Stra8-cre and $Becn1^{flox/flox}$ male mice. One cauda epididymis from each animal was cut into small fragments, and sperm were allowed to swim out in 500 mL of PBS for 30 min at 37°C under 5% CO₂. The sample was diluted in a 1:10 ratio and transferred to a hemocytometer for counting. The other cauda epididymis was used to measure sperm motility and velocity by computer-aided sperm analysis. For this purpose, the Zeiss Axio Scope A1 microscope (Carl Zeiss, Oberkochen, Germany) and accompanying LINE analysis software were employed. Non-fixed sperm were evenly spread on slides for morphological observation or immunostaining, dried at room temperature, fixed with 10% formalin for 20 min, and stained with the Diff-Quik Stain kit (Beijing Solarbio Science Technology, G1540) according to the manufacturer's instructions.

Immunofluorescence staining

For paraffin sections, testes and cauda epididymides were fixed in 4% paraformal dehyde (PFA) at 4°C overnight, dehydrated and embedded in paraffin. Sections of $5~\mu \rm m$ thickness were generated and then were mounted on glass slides and stained with hematoxylin. For frozen sections, testes were fixed in 4% PFA overnight at 4°C and dehydrated with 30% sucrose for 2 days. Testes were encased in optimal cutting temperature compound (Sakura, 4583) and quickly frozen in liquid nitrogen. Sections of 7 $\mu \rm m$ thickness were generated and mounted on glass slides.

Sections were microwaved in antigen retrieval buffer (10 mM sodium citrate, pH 6.0) for 15 min, cooled to room temperature, blocked, and permeated in 5% normal goat serum (Beyotime Biotechnology, C0265) for 1 h, followed by incubation with primary antibodies overnight at 4°C. After washing with PBS, the sections were incubated with secondary antibodies at 37°C for 1 h. After staining with 4′, 6-diamidino-2-phenylindole (Vectorlabs, H-1200-10), the sections were cover-slipped and observed with a Zeiss Scope A1 microscope.

Immunohistochemistry

Testes and cauda epididymides were obtained and fixed in 4% PFA at 4°C overnight, dehydrated, and embedded in paraffin. Sections of 5 μ m thickness were generated, mounted on glass slides, and deparaffinized. Sections were microwaved in antigen retrieval buffer as described above. Next, sections were saturated with endogenous peroxidase blockers to quench peroxidase activity, blocked, and permeated with 5% normal goat serum for 1 h, followed by incubation with primary antibodies overnight at 4°C. After washing with PBS, the sections were stained with Genzyme-conjugate goat antirabbit IgG polymer (Zhong Shan-Golden Bridge Biological Technology, PV-6001) for 1 h at 37°C. After staining with 3, 3-diaminobenzidine (Zhong Shan-Golden Bridge Biological Technology, PV-6001) and hematoxylin (Beyotime Biotechnology, C0105M), the sections were observed with the Zeiss Scope A1 microscope.

Western blotting

For protein extraction, the testes were homogenized with RIPA buffer (Beyotime Biotechnology, P0013B) containing a

protease inhibitor cocktail (Beyotime Biotechnology, P1005). Lysates were centrifuged for 30 min at 4°C, and the supernatants were collected. Protein concentrations were measured with the BCA assay kit (Beyotime Biotechnology, P0011). For western blotting, the proteins were separated by SDS-PAGE and electro-transferred to polyvinylidene fluoride membranes (Bio-Rad, 1620177). Membranes were incubated in 5% skim milk (Beijing Solarbio Science Technology, D8340) in 0.1% Tween-20 (Beijing Solarbio Science Technology, T8820)/Trisbuffered saline for 1.5 h to block nonspecific binding sites and incubated with primary and secondary antibodies. Immunoreactive proteins were detected using an enhanced chemiluminescence detection kit (Bio-Rad, 1709170) and visualized using a chemiluminescence imaging analysis system (Tanon 5200, Beijing, China) after washing membranes with 0.1% Tween-20/Tris-buffered saline. All the bands are in the linear range of detection.

Scanning electron microscopy

Epididymal sperm was obtained as described above, diluted, evenly smeared on glass slides, and air-dried. Cell smears were fixed with 2.5% glutaraldehyde for approximately 2 h. After washing with PBS, the samples were post-fixed with 2% OsO4 for 1 h at room temperature and dehydrated in a graded ethanol series. Cell smears were incubated with 100% propylene oxide (three changes, 10 min each), dried in a critical point dryer (EM CPD300, Leica, Germany), and sprayed with gold using an IB-3 ion coater (Eiko, Japan). The morphology of sperm was observed with a scanning electron microscope (Hitachi S-3400N, Hitachi, Tokyo, Japan).

Transmission electron microscopy

Testes and cauda epididymides were fixed in 2.5% glutaraldehyde for 24 h at 4°C. Testes were cut into 1 mm³ fragments and immersed in 1% OsO4 in 0.2 mM cacodylate buffer for 2 h at 4°C. Fixed tissues were dehydrated in a graded ethanol series and embedded in resin. Seminiferous tubules of stages IV–XII were selected on semi-thin sections, and ultra-thin sections were prepared. Cauda epididymides containing prominent lumens were selected for ultra-thin sectioning. Ultra-thin sections were stained with uranyl acetate and lead citrate and observed with a transmission electron microscope (Hitachi H-7500; Hitachi, Tokyo, Japan).

Statistical analysis

All data were analyzed with GraphPad Prism software. Student *t*-test was used to compare differences between two groups. One-way analysis of variance with Tukey post hoc test was used to compare differences among multiple groups. Results are presented as means \pm SEMs. Significance is noted as *P < 0.05, **P < 0.01.

Results

BECN1 is abundant in the mouse testis and mainly located in the cytoplasm of germ cells

BECN1 protein abundance in testes and other tissues of mice were examined by western blotting. As shown in Figure 1A, BECN1 protein was more abundant in testis than that in

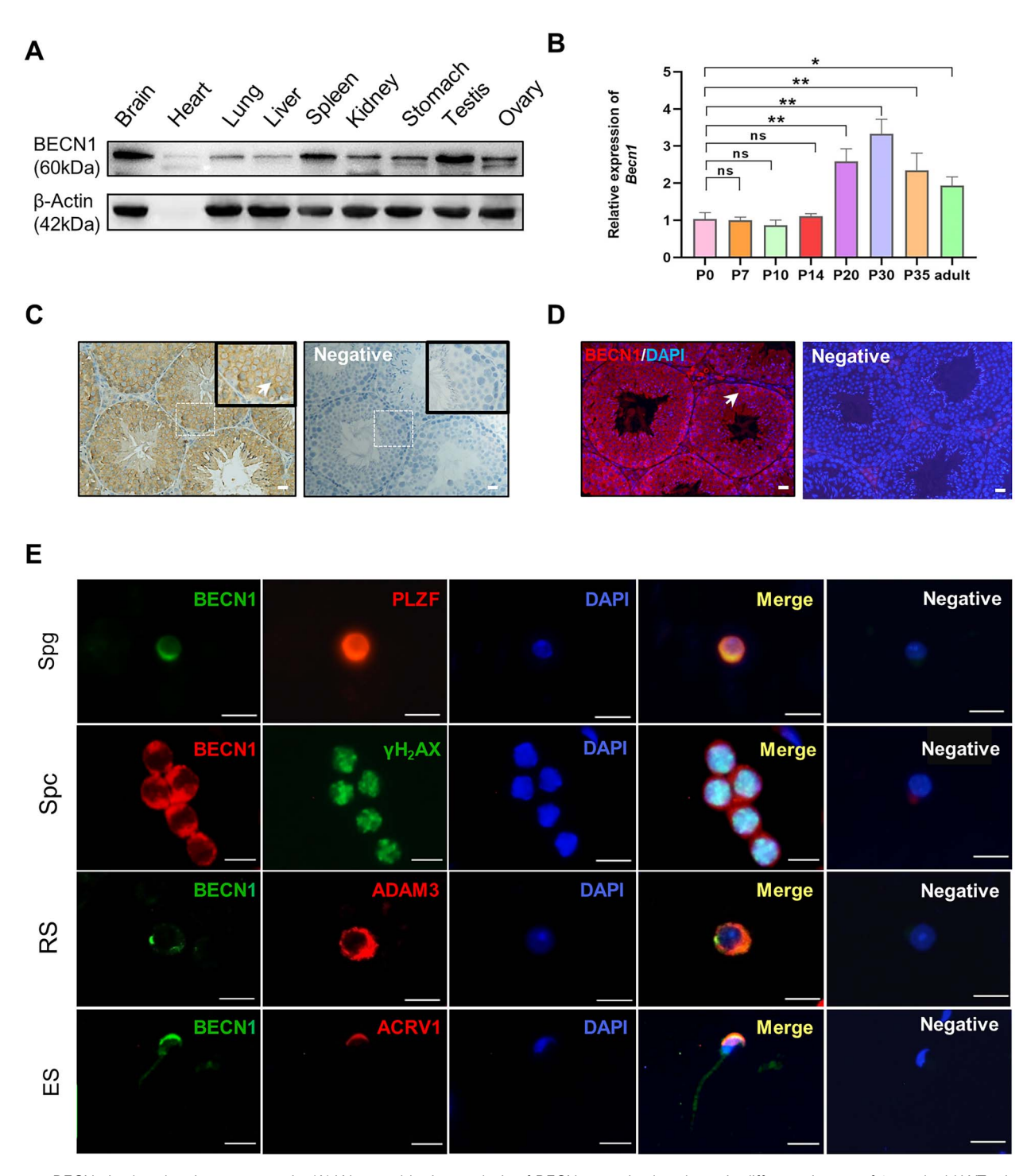


Figure 1. BECN1 is abundant in mouse testis. (A) Western blotting analysis of BECN1 protein abundance in different tissues of 8-week-old WT mice. β -Actin was used as a loading control. n=3. (B) Messenger RNA expression of Becn1 in WT mice from P0 to adult, P0 was set to 1. n=3; ns, no significance; *P < 0.05; **P < 0.05; **P < 0.01. (C, D) Immunohistochemistry (left) and immunofluorescence (right) staining of BECN1 in 8-week-old mouse testes. BECN1 is mainly located in the cytoplasm of spermatogenic cells (arrow). Negative, negative controls (primary-antibody-omitted sample). Scale bar = 10 μm. (E) Immunofluorescence staining of BECN1 in isolated male germ cells of 8-week-old mouse testes. The BECN1 protein was present in the cytoplasm of isolated spermatogonium (PLZF), spermatocyte (γ H2AX), round spermatid (ADAM3), and the acrosome and flagella of isolated elongating spermatid (ACRV1). Negative, negative controls (primary-antibody-omitted sample). Scale bar = 10 μm. ACRV1, acrosomal vesicle protein 1; ADAM3, a disintegrin and metalloproteinase 3; ES, elongating spermatid; γ H2AX, H₂A histone family member X; PLZF, promyelocytic leukemia zinc finger; Spg, spermatogonium; Spc, spermatocyte; RS, round spermatid; WT, wild type.

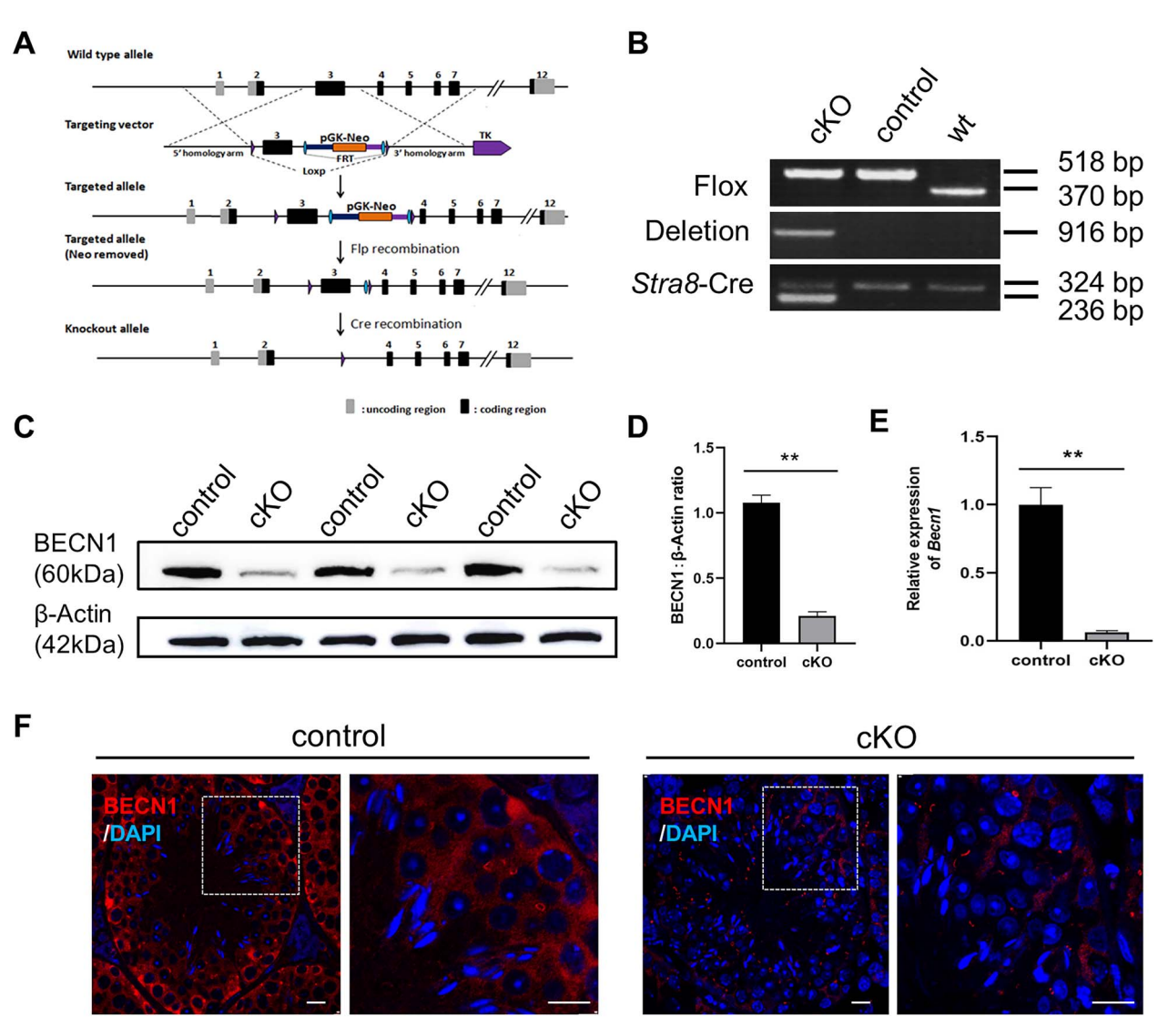


Figure 2. The generation of the cKO mice. (A) Schematic strategy for generation of Becn1 conditional knockout mice by deletion of exon 3 on mouse chromosome 11. The black triangles indicate the positions of the LoxP sites. (B) The genotyping of mice by PCR. Flox, 518 bp; wild-type, 370 bp; floxed after deletion, 916 bp; Stra8-internal control: 324 bp, Stra8-Cre: 236 bp. $Becn1^{flox/flox}$ was used as a loading control. (C) Representative brands of BECN1 protein abundance in control and cKO mice. β-Actin was used as a loading control. (D) Quantification of the relative BECN1 protein expression. n=3, **P < 0.01. (E) Becn1 mRNA expression was dramatically reduced in the testes of cKO mice. n=4, **P < 0.01. (F) Immunofluorescence staining results showed that BECN1 protein abundance was dramatically absent in testicular germ cells of 8-week-old cKO mice and was only presented in the cytoplasm of Sertoli cells. Boxed regions are magnified to the right. Scale bar = 20 μm (right or left).

lungs, liver, spleen, stomach, and ovaries (Figure 1A). Furthermore, spatiotemporal expression of Becn1 was performed by quantitative polymerase chain reaction (qPCR), and Becn1 mRNA expression was first detected on postnatal day 0 (P0) and markedly evaluated on P20 (Figure 1B), corresponding to the first appearance of round spermatids in seminiferous tubules. The elevated expression of Becn1 from P20 to adulthood may indicate an important role of Becn1 in spermiogenesis. Interestingly, immunohistochemistry and immunofluorescence staining of testicular sections showed that BECN1 was mainly located in the cytoplasm of germ cells (Figure 1C and D). To better define the cellular localization of BECN1, we performed co-immunofluorescence staining using isolated germ cells and found that BECN1 was localized predominantly in the cytoplasm of spermatogonia, spermatocytes, and round spermatids. After the removal of cytoplasm in elongating spermatids, BECN1 was mainly expressed in the acrosome and flagella midpiece of sperm (Figure 1E).

Generation of male germ cell–specific *Becn1* knockout mice

To investigate the role of BECN1 in the testis, we generated male germ cell-specific Becn1 knockout mice that were designated as Becn1flox/\Delta; Stra8-Cre mice (hereafter referred to as cKO mice). cKO mice were generated from the cross of Becn1flox/flox mice with Stra8-Cre mice. Becn1flox/flox mice were obtained by inserting two LoxP sites into exon 3 of the Becn1 gene (hereafter referred to as control mice), and the genotype of mice was identified by polymerase chain reaction (Figure 2A and B). The knockout efficiency of Becn1 in the testis of cKO mice was performed by detecting the mRNA expression and protein abundance. Results showed that BECN1 protein abundance in cKO mice were significantly lower than that in control mice (Figure 2C and D), and Becn1 mRNA levels in cKO mice were almost undetectable (Figure 2E). Immunofluorescence staining revealed that BECN1 expression was almost undetectable in the

Table 1. Fertility test of male mice

Mattings	No. of males tested	No. of fertile males	Average litters/male	Total pups/male
♂Control × ♀WT	7	7	3.57 ± 0.20^{a}	22.57 ± 2.20^{a}
$\sigma cKO \times \varphi WT$	7	7	1.14 ± 0.14^{b}	$5.29 \pm 0.68^{\mathrm{b}}$

Each male (2–4 months old) was engaged with two adult WT females. Average litters/male and total pups/male at birth were compared using Student t-test. Data are shown as mean \pm SEM. ^{a,b}Means in a column without a common superscript letter differ (P < 0.05).

cytoplasm of germ cells but detectable in the cytoplasm of Sertoli cells (Figure 2F). The expression of BECN1 in the cytoplasm of Sertoli cells may contribute to the low BECN1 protein abundance and *Becn1* mRNA expression in testes (Figure 2C–E). These results indicated that the generation of the model of male germ cell–specific *Becn1* knockout mice was successful.

Loss of *Becn1* in male germ cells leads to spermatozoa with low quantity and quality and reduced fertility

Most cKO mice survived and there were no differences in the testicular morphology and size between cKO mice and controls (Supplementary Figure S1A and B). However, the fertility of cKO mice was decreased after mating male mice with female WT mice for more than 2 months when compared with controls (Table 1). The sperm density in the epididymis was measured by quantitative analysis, and sperm motility was measured by computerassisted semen analysis. Correspondingly, sperm density $(4.17 \pm 0.28 \times 10^6 \text{ vs. } 9.88 \pm 0.89 \times 10^6)$, sperm motility $(26.84 \pm 2.84\% \text{ vs. } 86.91 \pm 0.84\%)$, progressive sperm rate $(3.13 \pm 0.31\% \text{ vs. } 29.58 \pm 1.47\%)$, sperm curvilinear velocity $(64.37 \pm 2.51 \ \mu\text{m/s} \text{ vs. } 15.68 \pm 1.14 \ \mu\text{m/s})$, sperm straight line velocity $(20.81 \pm 0.60 \ \mu \text{m/s} \text{ vs. } 3.98 \pm 0.31 \ \mu \text{m/s})$ and sperm average path velocity (29.52 \pm 0.84 μ m/s vs. $6.26 \pm 0.43 \ \mu\text{m/s})$ were all significantly impaired in cKO mice when compared with controls (Figure 3A–F).

Sperm morphology is closely related to sperm quality, so we stained cell smears using the Diff-Quik kit to observe the morphology of sperm. Sperm of cKO mice show a large number of morphological abnormalities (Supplementary Figure S1C and D). In control mice, sperm had normal sickleshaped heads and smooth flagella, but in cKO mice, sperm had deformed or missing heads, folded flagella principal piece, and flagella midpiece defects (Figure 3G). The abnormal sperm were counted, and the rate of malformed sperm heads in cKO mice $(39.93 \pm 1.69\%)$ was about 3.4 fold compared with control mice (11.76 \pm 2.22%), the rate of folded flagella principal piece in cKO mice $(18.55 \pm 3.51\%)$ was about 3.1-fold compared with control mice $(5.94 \pm 0.67\%)$, and the rate of defective flagella midpiece in cKO mice $(55.84 \pm 2.69\%)$ was about 13.2-fold compared with control mice $(4.23 \pm 0.27\%)$ (Figure 3H).

By scanning electron microscopy, we observed the ultrastructural abnormalities in the sperm of cKO mice. Compared with control mice, whose sperm heads and acrosomes were normal, the sperm heads in cKO mice were bent and broken (Figure 3Ii–iii). Compared with control mice, the flagella midpiece of sperm in cKO mice were incomplete and irregular, with most flagella midpiece swollen, exposing the intermediate axoneme structure (Figure 3Iiv–vi). Compared with control mice, the flagella principal piece of sperm in cKO mice were folded and coiled (Figure 3Ivii–ix). By transmission electron microscopy, the residual cytoplasm of cKO mice sperm was detected, which contained a nucleus forming the sperm head and mitochondria aggregated in the sperm tail (Figure 2J). Collectively, these results suggested that *Becn1* knockout in germ cell impaired the fertility of mice through reductions of sperm quality and quantity.

Deletion of *Becn1* in male germ cells leads to defective spermatogenesis and disrupted apical ectoplasmic specialization

Whether the reduction of sperm quantity is related to the apoptosis of spermatogenic cells in cKO mice was considered, so we assessed the apoptosis of spermatogenic cell by TUNEL assay on testis sections and found no change in the number of TUNEL-positive signals in cKO mice compared with control mice (Supplementary Figure S2A and B). However, periodic acid-Schiff (PAS) staining was performed to reveal severe disruptions of seminiferous epithelial cycles in cKO mice (Figure 4A). Compared with control mice, step-16 elongating spermatids were unsuccessfully released into the seminiferous tubule lumen in stages IX-XII in cKO mice (Figure 4A). Partial failure of spermiation may be the cause of the decrease in sperm quantity. Furthermore, other abnormalities included the detection of round head sperm and immature sperm in the cauda epididymis (Supplementary Figure S3A) and B).

We considered aberrant sperm morphology and the unsuccessful release of sperm during spermatogenesis in terms of the apical ectoplasmic specialization (ES), an anchoring device rich in F-actin that influences sperm motility, contributes to sperm head shaping, and facilitates sperm release [24, 25]. To determine the integrity of the apical ES, immunofluorescence staining and transmission electron microscopy were conducted to detect F-actin, an important component of the apical ES in Sertoli cells. In control mice, F-actin surrounded the tip of the sperm head, but in cKO mice, the apical ES showed morphological defects with disordered F-actin distribution and disorganized F-actin bundles (Figure 4B–D). Taken collectively, these results suggested that loss of *Becn1* may disrupt the cytoskeletal structure involving spermatogenesis.

Deletion of *Becn1* in male germ cells leads to acrosomal abnormalities

Due to sperm head defects observed on our previous findings and the fact that the role of autophagy in acrosome biogenesis has been reported [11–13], we explored the acrosome of sperm. Immunofluorescence staining of acrosomal vesicle protein 1 (ACRV1) was used to examine the morphology of acrosome and suggested that the sperm acrosome in cKO mice was anomalous or absent when compared with controls (Figure 5A and B). Next, transmission electron microscopy was used to detect the ultrastructure of sperm

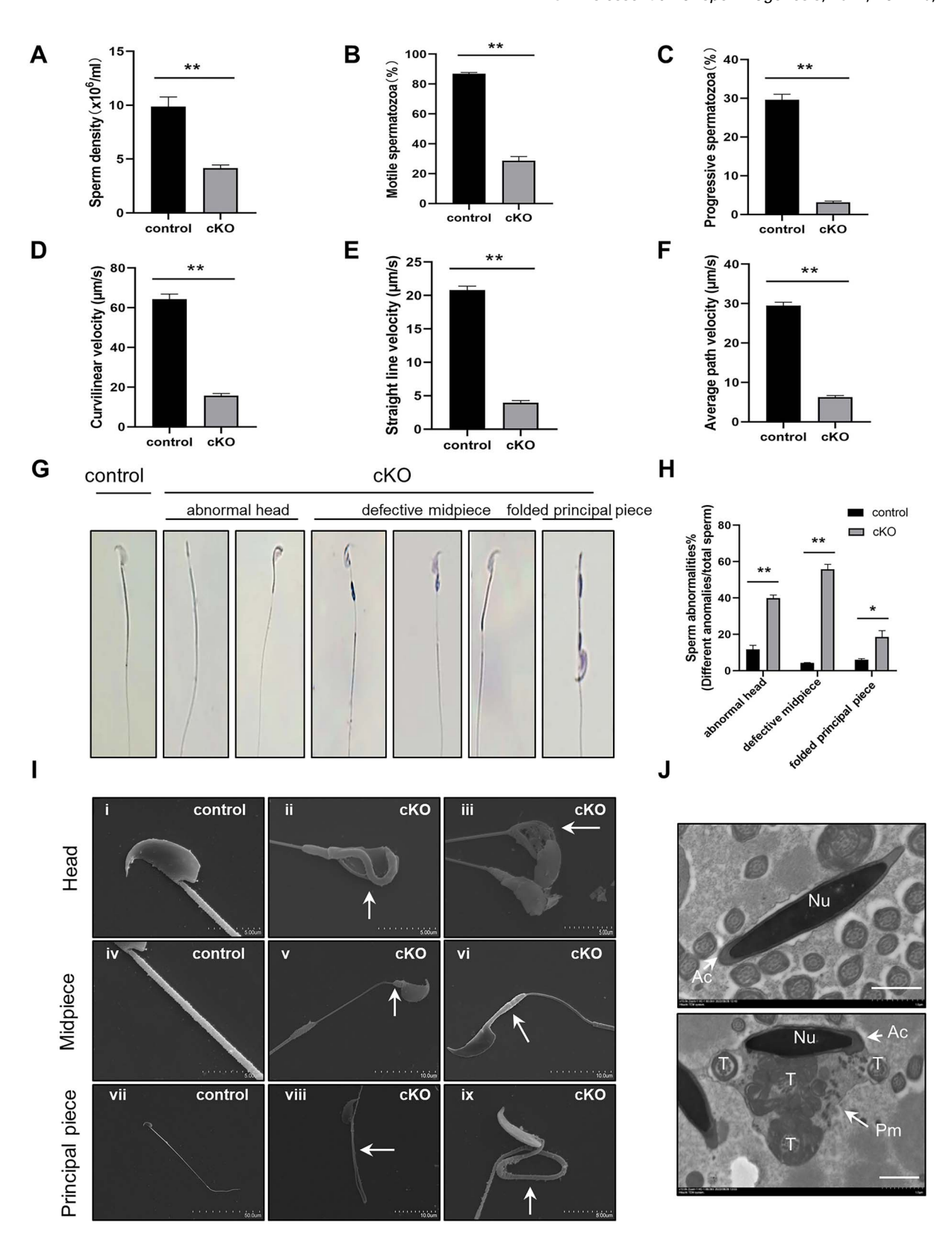


Figure 3. The defects of the cKO mice. (A) Sperm density of control and cKO mice, $9.88 \pm 0.89 \times 10^6$ vs. $4.17 \pm 0.28 \times 10^6$. n = 7, **P < 0.01. (B) Percentage of motile sperm of control and cKO mice, $86.91 \pm 0.84\%$ vs. $26.84 \pm 2.84\%$. n = 7, **P < 0.01. (C) Percentage of progressive sperm of control and cKO mice, $29.58 \pm 1.47\%$ vs. $3.13 \pm 0.31\%$. n = 7, **P < 0.01. (D) Curvilinear velocity of control and cKO mice, 64.37 ± 2.51 μm/s vs. 15.68 ± 1.14 μm/s. n = 7, **P < 0.01. (E) Straight line velocity of control and cKO mice, 20.81 ± 0.60 μm/s vs. 3.98 ± 0.31 μm/s. n = 7, **P < 0.01. (F) Average path velocity of control and cKO mice, 29.52 ± 0.84 μm/s vs. 6.26 ± 0.43 μm/s. n = 7, **P < 0.01. (G) Representative images of single normal sperm, abnormal head sperm, folded flagella principal piece sperm, and defective flagella midpiece sperm smears from control and cKO mice. (H) The statistical analysis of different types of abnormal sperm in the control and cKO mice. n = 4 (at least 300 sperm were randomly counted in each sample), *P < 0.05; **P < 0.01. (I) Scanning electron microscope for the ultrastructure of sperm. Arrows represent abnormalities. (J) Transmission electron microscope of sperm in lumen area of cauda epididymis of control and cKO mice. Scale bar = 1 μm. Nu, nucleus; Ac, acrosome; T, tail; Pm, plasma membrane.

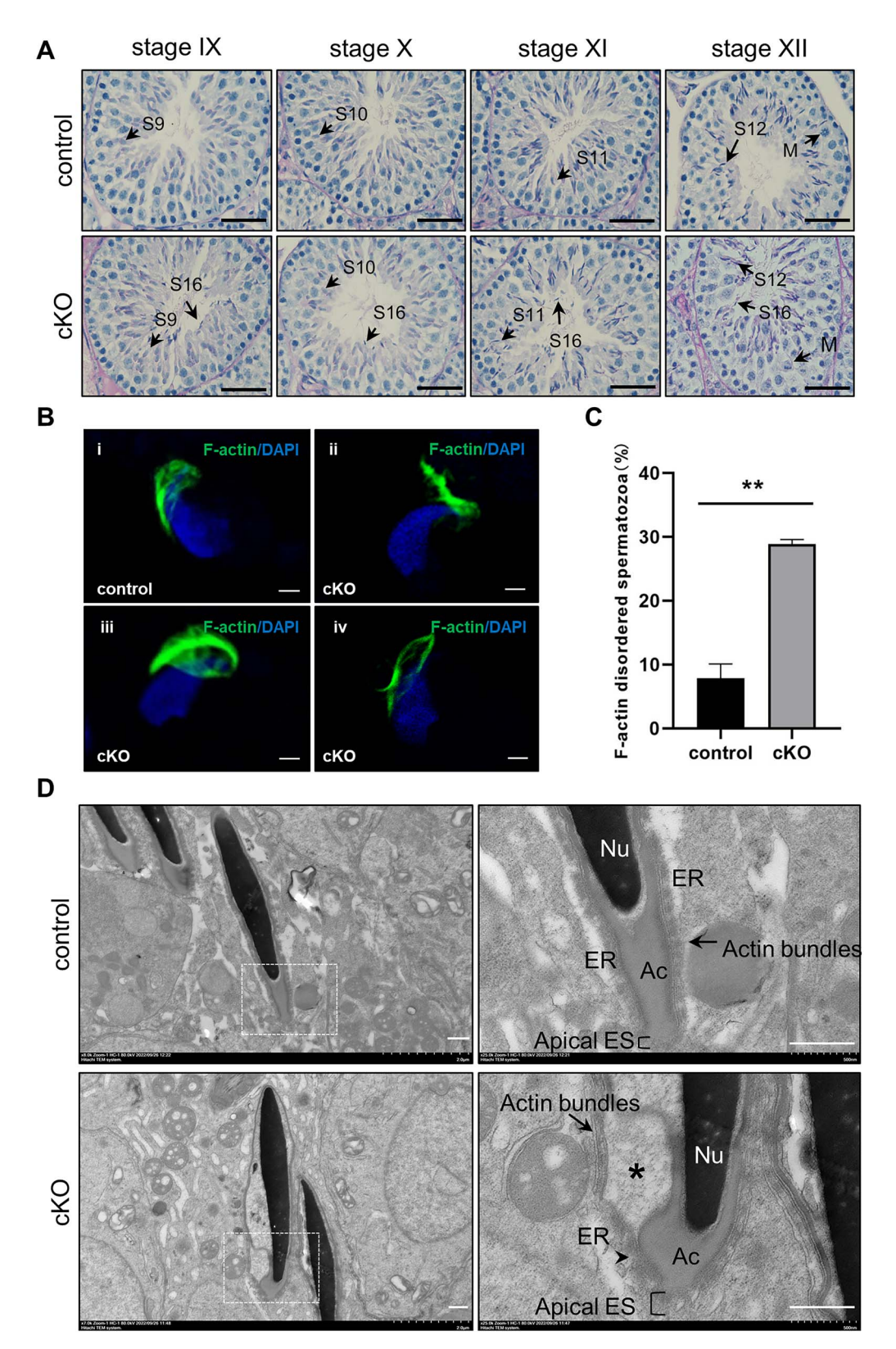


Figure 4. Defective spermatogenesis and apical ectoplasmic specialization in cKO mice. (A) PAS staining showing testis histology of the seminiferous tubules from control and cKO mice. S9/S10/S11/S12/S16, step 9/10/11/12/16 spermatid; step 16, spermatid indicates sperm that has not been released successfully at stage IX/X/XI/XII; M, meiotic divisions; Scale bar = $50 \mu m$. (B) Immunofluorescence staining of phalloidin (F-actin) of spermatids in control and cKO mice. Scale bar = $5 \mu m$. (C) The statistical analysis of F-actin disordered spermatozoa in control and cKO mice, $7.83 \pm 2.25\%$ vs. $28.85 \pm 0.72\%$. n=3 (at least 100 sperm were randomly counted in each sample), **P < 0.01. (D) Ultrastructural analysis of the apical ES in testis seminiferous tubules of control and cKO mice. Boxed regions are magnified to the right. Scale bar = $500 \mu m$. Arrows, the apical ES was characterized by the presence of actin bundles; Arrowhead, disordered actin bundles; asterisks: the structure of the apical ectoplasmic specialization was disrupted with large vacuoles; Nu, nucleus; Ac, acrosome; ER, endoplasmic reticulum.

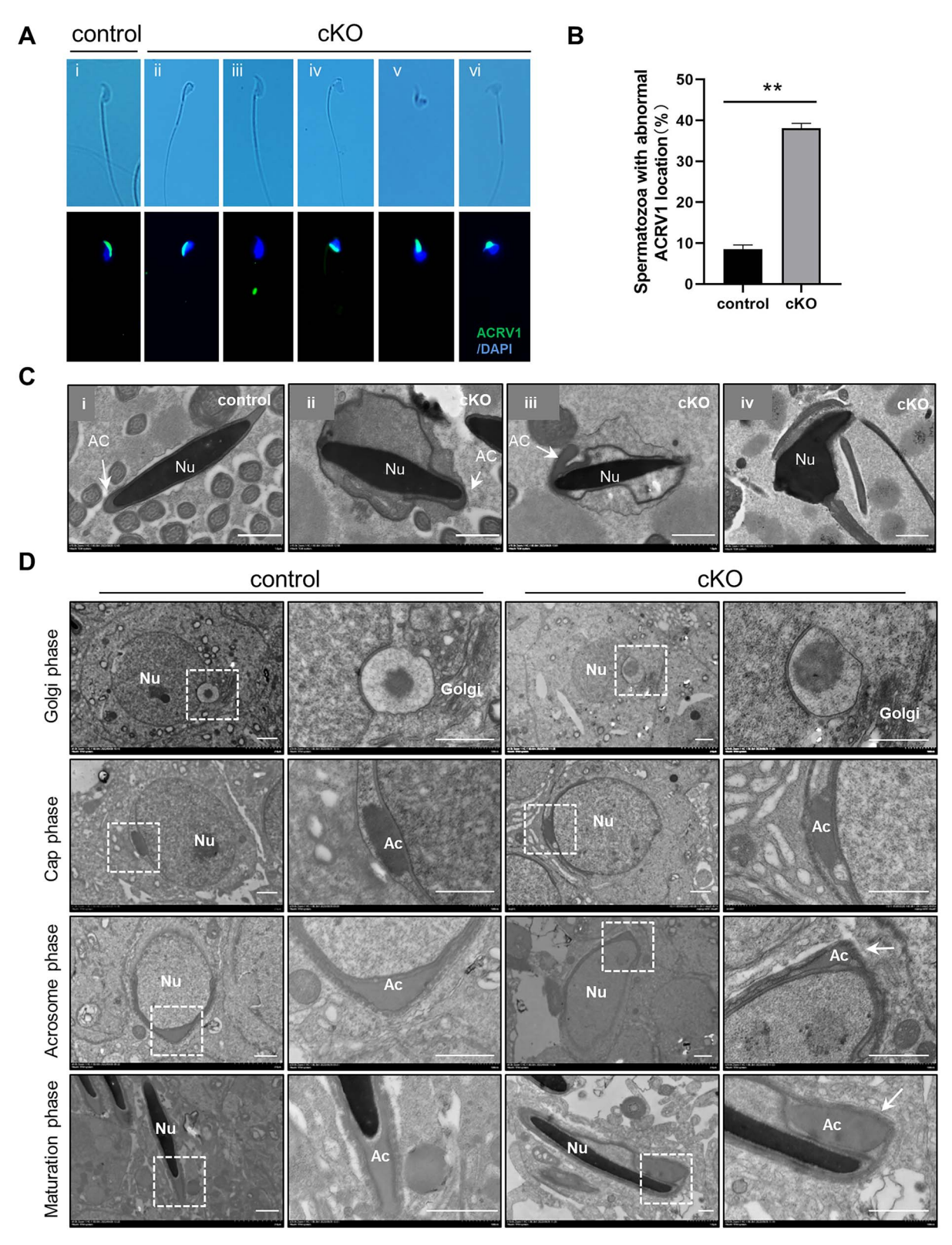


Figure 5. Deletion of Becn1 results in malformed acrosomes. (A) Immunofluorescence staining of sperm acrosome with ACRV1. i, normal acrosome; ii, folded head; iii, acrosome absence; iv–vi, malformed acrosome and fractured head. (B) The statistical analysis of spermatozoa with abnormal ACRV1 location in control and cKO mice, $8.58 \pm 0.97\%$ vs. $38.11 \pm 1.15\%$. n=3 (at least 100 sperm were randomly counted in each sample), **P < 0.01. (C) Transmission electron microscope for the ultrastructure of acrosome in cauda epididymis of control and cKO mice. i, normal acrosome; ii, separate acrosome; iii, irregular acrosome; iv, acrosome absence. Scale bar = 1 μ m. Nu, nucleus; Ac, acrosome; asterisk, vacuole. (D) Ultrastructural examination of acrosome biogenesis in seminiferous tubules of control and cKO mice. Boxed regions are magnified to the right. Scale bar = 1 μ m. Arrows represent defects. Nu, nucleus; Ac, acrosome; Golgi, Golgi body.

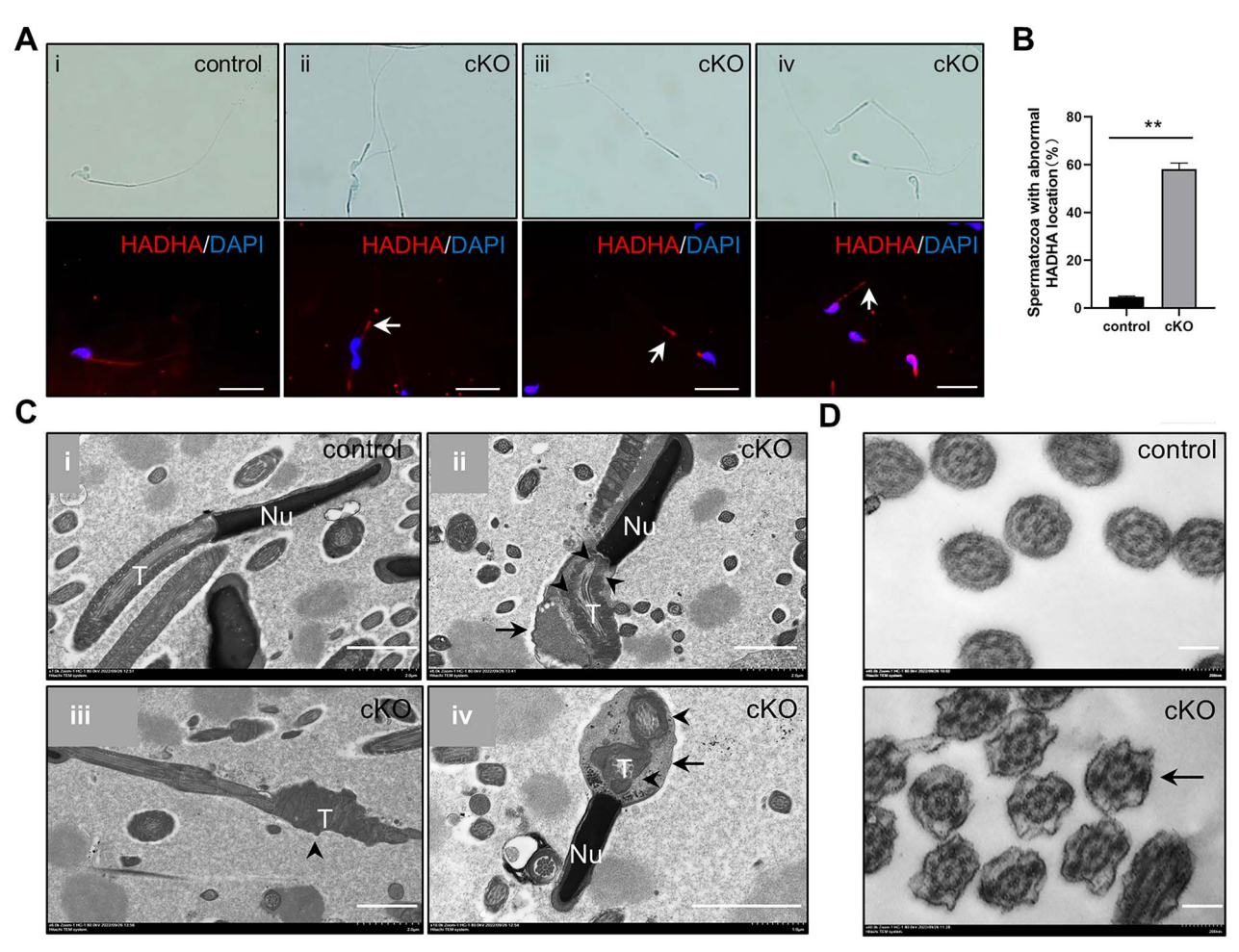


Figure 6. Deletion of Becn1 results in disrupted mitochondria and plasma membrane. (A) Immunofluorescence staining of sperm mitochondria with HADHA. i, normal mitochondria; ii–iii, mitochondria irregular accumulation (arrow); iv, flagella midpiece fragility (arrow). Scale bar = $20 \mu m$. HADHA, hydroxyacyl-CoA dehydrogenase trifunctional multienzyme complex subunit alpha. (B) The statistical analysis of spermatozoa with abnormal ACRV1 location in control and cKO mice, $4.66 \pm 0.38\%$ vs. $58.07 \pm 2.62\%$. n=3 (at least 100 sperm were randomly counted in each sample), **P < 0.01. (C) Transmission electron microscope illustrated aberrant distribution of mitochondria in cauda epididymis of cKO mice. Scale bar = $2 \mu m$. Arrow, plasma membrane; arrowhead, mitochondria aberrant distribution. Nu: nucleus; T: tails. (D) Transmission electron microscope illustrated loose plasma membrane in testis seminiferous tubules of cKO mice (arrow). Scale bar = 200 nm.

acrosome. Results indicated that the acrosomes were separated from the nucleus, irregular or absent in cKO mice (Figure 5C). Furthermore, considering the four phases of acrosome biogenesis, abnormalities were founded in the acrosome phase and maturation phase but not in the Golgi phase and cap phase in cKO mice by transmission electron microscopy. In the acrosome phase and the mature phase, the acrosome performed anomalous localization and morphology, which mainly manifested as the acrosome deviated from the apex of the nucleus and shaped irregularly (Figure 5D). Thus, loss of *Becn1* may mainly affect the later stages of spermiogenesis.

Deletion of *Becn1* in male germ cells disrupted mitochondrial sheath in sperm

Mitochondria, located in the midpiece of the flagella, are one of the few organelles that remain during spermiogenesis and mediate sperm motility. Mitochondria were stained with hydroxyacyl-CoA dehydrogenase trifunctional multienzyme complex subunit alpha (HADHA), and aberrant distribution of mitochondria in the flagella midpiece was observed in cKO mice (Figure 6A and B). In consistency with mitochondria staining, malformed mitochondrial sheath in

the flagella midpiece was observed by transmission electron microscopy (Figure 6C). Correspondingly, mitochondria of control mice were neatly arranged around the axoneme (Figure 6Ci), but mitochondria of cKO mice were arranged abnormally, with overlapping and stacking or missing structures (Figure 6Cii–iv). The failure of residual cytoplasm shedding in the flagella of cKO mice may be associated with the abnormal flagellum development (Figure 6Civ). Additionally, loose plasma membranes were observed at the flagella endpiece of sperm in cKO mice (Figure 6D). These results indicated that loss of *Becn1* affected the biogenesis of sperm flagella.

Deletion of *Becn1* leads to a disrupted autophagy flux in the testis

The role of BECN1, a core factor of autophagy, in sperm abnormalities induced by autophagy was examined. Compared with control mice testes, the autophagic receptor and substrate SQSTM1/p62 was accumulated, and autophagy core protein ATG5 was reduced in cKO mice testes. In addition, LC3-I but not the membrane-associated form LC3-II was accumulated in cKO mice testes (Figure 7A–D).

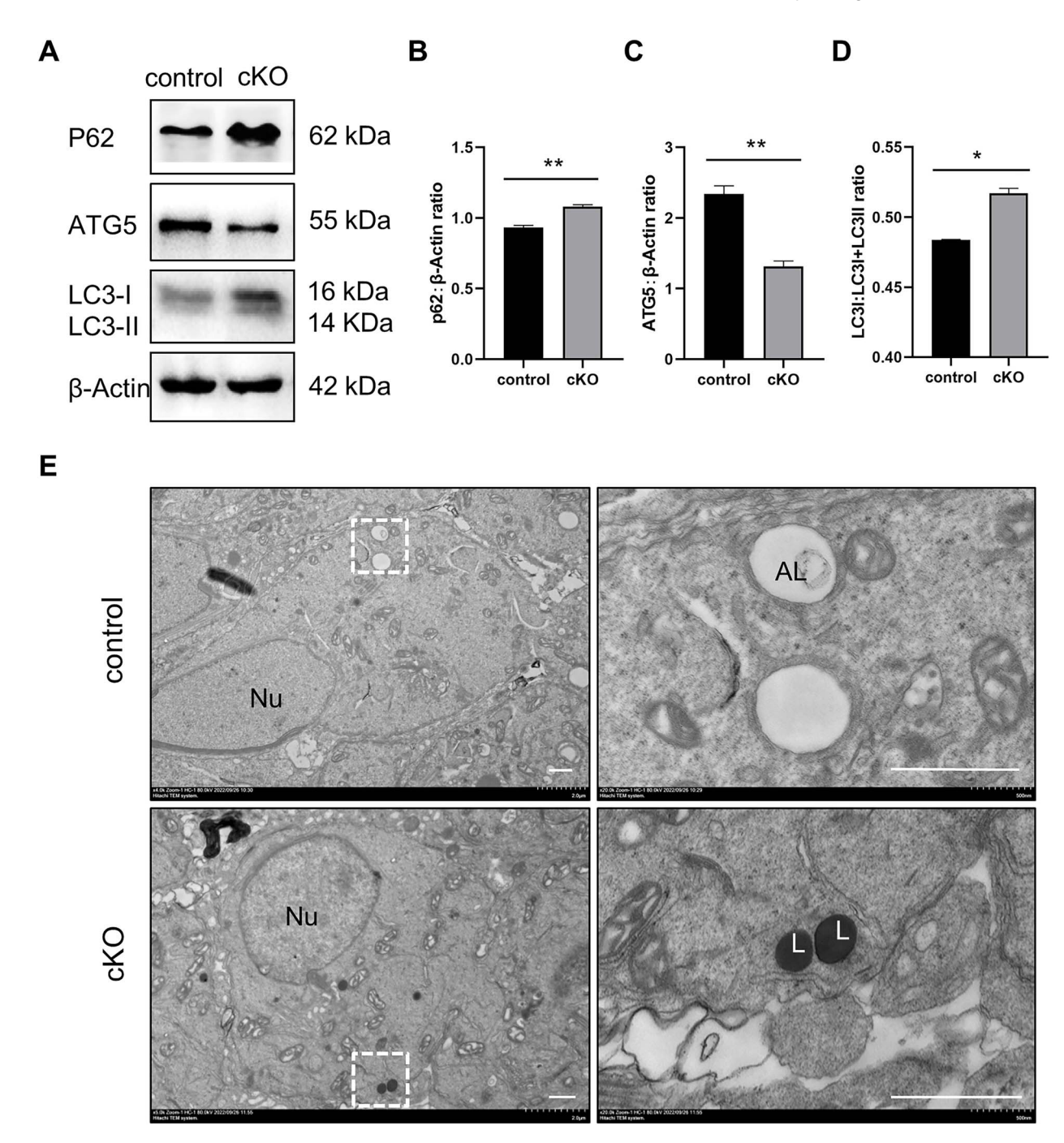


Figure 7. Deletion of Becn1 results in disrupted autophagic flux. (A) Representative western blotting of p62, ATG5, and LC3-I/II in control and cKO mice. β-Actin was used as a loading control. n = 3. (B–D) Statistical analysis of protein abundances of p62, ATG5 and LC3-I/II in control and cKO mice. n = 3, *P < 0.05, **P < 0.01. (E) Transmission electron microscope of lumen area of seminiferous tubules of control and cKO mice. Boxed regions are magnified to the right. Scale bar = 1 μm. Nu, nucleus; AL, autolysosome; L, lysosome.

Interestingly, the number of lysosomes increased and the number of autolysosomes decreased in cKO mice testes (Figure 7E), suggesting that autophagy flux may be disrupted in cKO mice.

Discussion

Autophagy is an evolutionarily conserved self-digestion process that is required for the maintenance of cellular homeostasis [26]. Growing studies demonstrated that autophagy plays a

key role in spermatogenesis [11, 13, 27], hormonal regulation [21, 28, 29], and genital system diseases [9]. BECN1 is a key regulator of autophagy, and it has been reported to maintain spermatocyte quantity and to affect spermatogenesis and testicular function in mice under external stress [30, 31]. However, the role of BECN1 in male spermatogenesis is largely unknown. In the present study, male germ cell–specific *Becn1* knockout mice were generated to explore the role of BECN1 in male spermatogenesis.

BECN1 is highly expressed in the testes, indicating its potential role in spermatogenesis. *Becn1* mRNA expression

significantly increased in testis on postnatal day 20 (P20), which corresponds to the first appearance of round spermatids (i.e., during the first round of spermatogenesis) in mice [32] and remained elevated on P30, P35, and adult. Furthermore, immunofluorescence experiments revealed that BECN1 was mainly localized in the cytoplasm of spermatogenic cells, acrosome, and flagella midpiece after cytoplasmic detachment, suggesting that BECN1 is closely associated with spermiogenesis, a process that involves extensive morphological changes such as the degradation of cytoplasmic components, rearrangement of mitochondria, and development of flagella and acrosomes [33]. To investigate the role of *Becn1* in male reproduction, we used the Cre/LoxP system to knockout the Becn1 because of death occurred in early embryonic day (E) 7.5 or earlier of Becn1 null mice development [19]. The Cre activity of Stra8-Cre transgenic mice was first detected in prospermia of P3 testes, and Cre expression continued until the preleptotene spermatocyte stage [34], which is a good system for germ cell-specific knockout of specific genes in mice. Furthermore, recombination efficiency of the Cre/LoxP system in specific cell lines, the selection of appropriate germlinespecific Cre transgenic mouse lines as well as a reasonable mating scheme must be taken into consideration to obtain the cKO mice of high excision efficiency [35, 36]. These findings form the cornerstone of this study.

As we have seen, there was no significant difference in the size of the testes between cKO mice and control mice, the markedly reduced quantity and quality of sperm contribute to the reduced fertility. Moreover, although BECN1 is closely associated with apoptosis [37], sperm apoptosis is not the cause of sperm count decline in the testes of cKO mice; however, some sperm failed to release into the seminiferous tubule lumen, resulting in partial failure of spermatogenesis, which may contribute to the reduced sperm count in the cauda epididymis. Morphological observation of sperm revealed the presence of abnormalities in sperm heads, excessive residual cytoplasm, disorganized mitochondria, and decreased sperm motility of cKO mice, which is in agreement with deficiencies of other *Atg* conditional knockout mice [11, 13, 38].

To investigate the role of *Becn1* in spermiation, we examined the apical ES located at the Sertoli cell-elongated spermatid interface that regulates spermiation, sperm motility, and sperm head shaping [24, 25, 39]. The Sertoli ES is composed of three layers, a parallel actin bundles located between plasma membranes and cisternae of endoplasmic reticulum (ER) in the Sertoli cell [40]. Although the apical ES is a Sertoli cellspecific structure, the F-actin bundles surround the apex of the elongated spermatid nucleus and elongated spermatids express apical ES proteins similar to the ones expressed by Sertoli cells [40, 41], apical ES may not a complete Sertoli cell structure. F-actin surrounding the elongated spermatid nucleus, an essential component of the apical ES, is used to detect apical ES [42]. Previous studies reported that Factin was disordered in the apex region of elongated spermatid nucleus of germ cell–specific Atg7 knockout mice [27]. Consistently, we found that F-actin disruption was present in cKO mice, suggesting a relationship between autophagy and cytoskeletal dynamics. These findings indicate that apical ES function requires the joint action of Sertoli cells and spermatids.

Cytoskeletal components play an important role in the removal of residual cytoplasm. Effective cytoplasmic removal mainly mediated by Sertoli cells through engulfment, which is critical for sperm motility [43, 44]. The apical tubulobulbar complexes (TBCs) in Sertoli cells is an actin-based cytoskeletal structure [45], the role of apical TBC in facilitating removal of excess cytoplasm that is absorbed by adjacent Sertoli cells is considered important [46, 47]. The function of germ cells in regulating cytoplasmic removal has also been studied. PDZ and LIM domain protein 1 (PDLIM1), a negative regulator of cytoskeletal organization, was demonstrated to mediate the relationship between autophagy and cytoskeletal organization [27]. Disruption of autophagy leads to the accumulation of PDLIM1 in the cytoplasm, which affects cytoskeletal dynamics. Furthermore, autophagy disruption also leads to ineffective removal of cytoplasm during spermatogenesis, which indicates the key role of autophagy in regulating cytoplasmic removal in germ cells. Correspondingly, the levels of the autophagy core proteins microtubuleassociated protein 1 light chain 3 (LC3) and ATG7 are significantly increased in round to elongated spermatids [27, 48]. During this period from round to elongated spermatids, the numbers of lysosomes and autophagosomes increased, suggesting that autophagy may be involved in some related process in elongated spermatids. Similar to our observations in germ cell–specific *Becn1* knockout mice, compelling studies reported that the presence of residual cytoplasm in sperm from germ cell-specific Atg5 or Atg7 knockout mice was observed [11, 27]. Taken collectively, these findings suggest an important role of autophagy in the degradation and recycling of cytoplasmic components for maintaining the homeostasis of germ cells.

The sperm acrosome is a Golgi complex-derived flat granule, and it has been proposed to have originated from the lysosome. BECN1 has been reported to be localized in the acrosome of round spermatids [13]. In the present study, Becn1 expression can be found in the acrosome of elongated spermatids. Thus, we postulated that BECN1 affects acrosome development, which is supported by our results of abnormal acrosome biogenesis in germ cell-specific Becn1 knockout mice. Growing studies have suggested that autophagy plays a key role in sperm acrosome biogenesis [49-51] and loss of autophagy-related genes disrupts autophagy flux resulting in abnormalities of the acrosome in mice [11, 13]. For example, germ cell–specific Atg5 knockout mice exhibit acrosome abnormalities [11], and germ cell-specific Atg7 knockout mice display failed fusion of multiple acrosomal vesicles at the Golgi phase of acrosome development, which subsequently lead to acrosome malformations [13]. In comparison with ATG7, BECN1 tends to exert a more pronounced effect on acrosomal localization and morphology in the later phases of the acrosome biogenesis rather than the process of vesicle fusion in the early phases of acrosome biogenesis, involvement of BECN1 in a different stage of autophagy that may contribute to the different role of BECN1 and ATG7 in acrosome biogenesis.

During spermatogenesis, mitochondria are one of the few organelles retained in sperm, which undergo reduction and rearrangement to form mitochondrial sheaths packed tightly in the middle segment of the flagellum [52]. Although the mechanisms of the regulation of mitochondrial dynamics during spermatogenesis remain unclear, the coordinated action of multiple proteins involved in mitochondrial dynamics was reported [53–57]. The role of cytoskeletal proteins in mitochondrial transport and localization can cause abnormal mitochondrial aggregation in a microtubule-dependent

manner as was shown for kinesin light chain 3 (KLC3) [53, 54]. Additionally, mitochondrial membrane proteins and the members of dynamin family can mediate mitochondrial fusion and fission [55, 56]. Some proteins specific to spermatogenesis are also involved in mitochondrial regulation, such as spermatogenesis-associated 19 (SPATA19), which regulates mitochondrial organization and function and affect sperm viability, and spermatogenesis-associated 18 (SPATA18), which plays an important role in mitochondria quality control in cryopreserved spermatozoa [57, 58]. Interestingly, mitochondrial structural abnormalities were identified in germ cell-specific Becn1 knockout mice in our present study. This finding was similar to that observation in germ cellspecific Atg5 knockout mice [11], suggesting the key role of autophagy in mitochondrial reassembly. However, further studies are needed to understand the underlying mechanism of autophagy in the regulation of mitochondrial rearrangement.

Our understanding of BECN1 should go beyond its role in autophagy. For example, disruption of ATG6 (a homolog of Becn1) can affect pollen germination and male fertility through non-autophagic pathways in Arabidopsis [59]. BECN1 is involved in many different signaling pathways, including apoptosis, endocytosis, and cytoplasmic division [60-64]. Therefore, the mechanistic action of BECN1 in male mouse germ cells may be regulated in multiple ways, which requires additional in-depth studies. In the present study, disordered spermatogenesis resulting from disrupted autophagy was observed in germ cell-specific Becn1 knockout mice. Furthermore, residual cytoplasm, abnormal acrosome morphology, and abnormal mitochondrial accumulation were documented in sperm of Becn1 knockout mice, all of which affected sperm motility and quantity, leading to reduced fertility.

Abbreviations

ACRV1, acrosomal vesicle protein 1; ATG, autophagy-related; ES, ectoplasmic specialization; PAS, periodic acid–Schiff; PCR, polymerase chain reaction; Ptdlns3K, class III phosphatidylinositol 3-kinase; PFA, paraformaldehyde; qPCR, quantitative polymerase chain reaction; *Stra8*, stimulated by retinoic acid 8; SEM, scanning electron microscope; TBCs, tubulobulbar complexes; WT, wild type

Supplementary material

Supplementary material is available at BIOLRE online.

Conflict of interest

The authors have declared that no conflict of interest exists.

Ethics statement

All the animal experimental procedures were approved by the Institutional Animal Care and Use Committee of China Agricultural University.

Authors' contributions

All authors contributed to the study conception and design. Material preparation, samples collection, data analysis, and first draft writing were performed by LK and NL. Article guidance and revisions were done by NL and YQ. Sample collection was assisted by YW, XL, YL, ST, CY, and YH. All the authors approved the final version.

Data availability

All data and figure generated or used during the study appear in the submitted article.

References

- 1. Hess RA, Renato de Franca L. Spermatogenesis and cycle of the seminiferous epithelium. *Adv Exp Med Biol* 2008; **636**:1–15.
- de Kretser DM, Loveland KL, Meinhardt A, Simorangkir D, Wreford N. Spermatogenesis. Hum Reprod 1998; 13:1–8.
- 3. Wang M, Zeng L, Su P, Ma L, Zhang M, Zhang YZ. Autophagy: a multifaceted player in the fate of sperm. *Hum Reprod Update* 2022; 28:200–231.
- 4. Yang Z, Klionsky DJ. Eaten alive: a history of macroautophagy. *Nat Cell Biol* 2010; **12**:814–822.
- Glick D, Barth S, Macleod KF. Autophagy: cellular and molecular mechanisms. *J Pathol* 2010; 221:3–12.
- Mizushima N, Yoshimori T, Ohsumi Y. The role of Atg proteins in autophagosome formation. *Annu Rev Cell Dev Biol* 2011; 27: 107–132.
- 7. Kang R, Zeh HJ, Lotze MT, Tang D. The Beclin 1 network regulates autophagy and apoptosis. *Cell Death Differ* 2011; **18**:571–580.
- 8. Mizushima N, Komatsu M. Autophagy: renovation of cells and tissues. *Cell* 2011; 147:728–741.
- Zhu Y, Yin Q, Wei D, Yang Z, Du Y, Ma Y. Autophagy in male reproduction. Syst Biol Reprod Med 2019: 65:265–272.
- 10. Abraham MC, Shaham S. Death without caspases, caspases without death. *Trends Cell Biol* 2004; 14:184–193.
- 11. Huang Q, Liu Y, Zhang S, Yap YT, Li W, Zhang D, Gardner A, Zhang L, Song S, Hess RA, Zhang Z. Autophagy core protein ATG5 is required for elongating spermatid development, sperm individualization and normal fertility in male mice. *Autophagy* 2021; 17:1753–1767.
- Liu C, Wang H, Shang Y, Liu W, Song Z, Zhao H, Wang L, Jia P, Gao F, Xu Z, Yang L, Gao F, et al. Autophagy is required for ectoplasmic specialization assembly in sertoli cells. Autophagy 2016; 12:814–832.
- 13. Wang H, Wan H, Li X, Liu W, Chen Q, Wang Y, Yang L, Tang H, Zhang X, Duan E, Zhao X, Gao F, *et al.* Atg7 is required for acrosome biogenesis during spermatogenesis in mice. *Cell Res* 2014; 24:852–869.
- 14. Ma M, Liu JJ, Li Y, Huang Y, Ta N, Chen Y, Fu H, Ye MD, Ding Y, Huang W, Wang J, Dong MQ, et al. Cryo-EM structure and biochemical analysis reveal the basis of the functional difference between human PI3KC3-C1 and -C2. Cell Res 2017; 27:989–1001.
- Kaur G, Mital P, Dufour JM. Testisimmune privilege—assumptions versus facts. *Anim Reprod* 2013; 10:3–15.
- Yue Z, Zhong Y. From a global view to focused examination: understanding cellular function of lipid kinase VPS34-Beclin 1 complex in autophagy. J Mol Cell Biol 2010; 2:305–307.
- 17. Liang XH, Kleeman LK, Jiang HH, Gordon G, Goldman JE, Berry G, Herman B, Levine B. Protection against fatal Sindbis virus encephalitis by beclin, a novel Bcl-2-interacting protein. *J Virol* 1998; 72:8586–8596.
- Kihara A, Kabeya Y, Ohsumi Y, Yoshimori T. Beclinphosphatidylinositol 3-kinase complex functions at the trans-Golgi network. EMBO Rep 2001; 2:330–335.
- Yue Z, Jin S, Yang C, Levine AJ, Heintz N. Beclin 1, an autophagy gene essential for early embryonic development, is a haploinsufficient tumor suppressor. *Proc Natl Acad Sci U S A* 2003; 100: 15077–15082.

- Gawriluk TR, Ko C, Hong X, Christenson LK, Rucker EB 3rd. Beclin-1 deficiency in the murine ovary results in the reduction of progesterone production to promote preterm labor. *Proc Natl Acad Sci U S A* 2014; 111:E4194–E4203.
- Li WR, Chen L, Chang ZJ, Xin H, Liu T, Zhang YQ, Li GY, Zhou F, Gong YQ, Gao ZZ, Xin ZC. Autophagic deficiency is related to steroidogenic decline in aged rat Leydig cells. *Asian J Androl* 2011; 13:881–888.
- Zhang S, Liu Y, Huang Q, Yuan S, Liu H, Shi L, Yap YT, Li W, Zhen J, Zhang L, Hess RA, Zhang Z. Murine germ cell-specific disruption of Ift172 causes defects in spermiogenesis and male fertility. Reproduction 2020; 159:409–421.
- Morrow CM, Tyagi G, Simon L, Carnes K, Murphy KM, Cooke PS, Hofmann MC, Hess RA. Claudin 5 expression in mouse seminiferous epithelium is dependent upon the transcription factor ets variant 5 and contributes to blood-testis barrier function. *Biol Reprod* 2009; 81:871–879.
- Mruk DD, Silvestrini B, Cheng CY. Anchoring junctions as drug targets: role in contraceptive development. *Pharmacol Rev* 2008; 60:146–180.
- Toyama Y, Maekawa M, Yuasa S. Ectoplasmic specializations in the Sertoli cell: new vistas based on genetic defects and testicular toxicology. *Anat Sci Int* 2003; 78:1–16.
- Galluzzi L, Baehrecke EH, Ballabio A, Boya P, Bravo-San Pedro JM, Cecconi F, Choi AM, Chu CT, Codogno P, Colombo MI, Cuervo AM, Debnath J, et al. Molecular definitions of autophagy and related processes. EMBO J 2017; 36:1811–1836.
- Shang Y, Wang H, Jia P, Zhao H, Liu C, Liu W, Song Z, Xu Z, Yang L, Wang Y, Li W. Autophagy regulates spermatid differentiation via degradation of PDLIM1. *Autophagy* 2016; 12: 1575–1592.
- Beattie MC, Adekola L, Papadopoulos V, Chen H, Zirkin BR. Leydig cell aging and hypogonadism. *Exp Gerontol* 2015; 68: 87–91.
- Gao F, Li G, Liu C, Gao H, Wang H, Liu W, Chen M, Shang Y, Wang L, Shi J, Xia W, Jiao J, et al. Autophagy regulates testosterone synthesis by facilitating cholesterol uptake in Leydig cells. J Cell Biol 2018; 217:2103–2119.
- 30. Yin J, Ni B, Yang YD, Tang ZW, Gao ZQ, Feng L, Liao WG, Gao YQ. Elevation of autophagy rescues spermatogenesis by inhibiting apoptosis of mouse spermatocytes. *Reproduction* 2018; **156**: 545–558.
- 31. Huang W, Cao Z, Zhang J, Ji Q, Li Y. Aflatoxin B(1) promotes autophagy associated with oxidative stress-related PI3K/AKT/mTOR signaling pathway in mice testis. *Environ Pollut* 2019; 255:113317.
- Kurohmaru M, Sinha Hikim AP, Mayerhofer A, Bartke A, Russell LD. Golden hamster myoid cells during active and inactive states of spermatogenesis: correlation of testosterone levels with structure. Am J Anat 1990; 188:319–327.
- 33. Tanaka H, Baba T. Gene expression in spermiogenesis. *Cell Mol Life Sci* 2005; **62**:344–354.
- Sadate-Ngatchou PI, Payne CJ, Dearth AT, Braun RE. Cre recombinase activity specific to postnatal, premeiotic male germ cells in transgenic mice. *Genesis* 2008; 46:738–742.
- 35. Bao J, Ma HY, Schuster A, Lin YM, Yan W. Incomplete Cremediated excision leads to phenotypic differences between Stra8-iCre; Mov10l1(lox/lox) and Stra8-iCre; Mov10l1(lox/Delta) mice. *Genesis* 2013; 51:481–490.
- Rodriguez JD, Myrick DA, Falciatori I, Christopher MA, Lee TW, Hannon GJ, Katz DJ. A model for epigenetic inhibition via transvection in the mouse. *Genetics* 2017; 207: 129–138.
- Djavaheri-Mergny M, Maiuri MC, Kroemer G. Cross talk between apoptosis and autophagy by caspase-mediated cleavage of Beclin 1. Oncogene 2010; 29:1717–1719.
- 38. Aparicio IM, Espino J, Bejarano I, Gallardo-Soler A, Campo ML, Salido GM, Pariente JA, Pena FJ, Tapia JA. Autophagy-related proteins are functionally active in human spermatozoa and may

- be involved in the regulation of cell survival and motility. *Sci Rep* 2016: 6:33647.
- Mruk DD, Cheng CY. Cell-cell interactions at the ectoplasmic specialization in the testis. *Trends Endocrinol Metab* 2004; 15: 439–447.
- 40. Vogl AW, Pfeiffer DC, Mulholland D, Kimel G, Guttman J. Unique and multifunctional adhesion junctions in the testis: ectoplasmic specializations. *Arch Histol Cytol* 2000; 63:1–15.
- 41. Kopera IA, Bilinska B, Cheng CY, Mruk DD. Sertoli-germ cell junctions in the testis: a review of recent data. *Philos Trans R Soc Lond B Biol Sci* 2010; 365:1593–1605.
- 42. Lie PP, Mruk DD, Lee WM, Cheng CY. Cytoskeletal dynamics and spermatogenesis. *Philos Trans R Soc Lond B Biol Sci* 2010; **365**: 1581–1592.
- 43. Ahmed N, Yufei H, Yang P, Muhammad Yasir W, Zhang Q, Liu T, Hong C, Lisi H, Xiaoya C, Chen Q. Cytological study on Sertoli cells and their interactions with germ cells during annual reproductive cycle in turtle. *Ecol Evol* 2016; 6:4050–4064.
- 44. Carr I, Clegg EJ, Meek GA. Sertoli cells as phagocytes: an electron microscopic study. *J Anat* 1968; 102:501–509.
- Mruk DD, Cheng CY. Sertoli-Sertoli and Sertoli-germ cell interactions and their significance in germ cell movement in the seminiferous epithelium during spermatogenesis. *Endocr Rev* 2004; 25: 747–806.
- Russell LD. Spermatid-Sertoli tubulobulbar complexes as devices for elimination of cytoplasm from the head region late spermatids of the rat. Anat Rec 1979; 194:233–246.
- 47. Upadhyay RD, Kumar AV, Ganeshan M, Balasinor NH. Tubulobulbar complex: cytoskeletal remodeling to release spermatozoa. *Reprod Biol Endocrinol* 2012; **10**:27.
- 48. Yang P, Ahmed N, Wang L, Chen H, Waqas Y, Liu T, Haseeb A, Bangulzai N, Huang Y, Chen Q. In vivo autophagy and biogenesis of autophagosomes within male haploid cells during spermiogenesis. *Oncotarget* 2017; 8:56791–56801.
- 49. Liu C, Song Z, Wang L, Yu H, Liu W, Shang Y, Xu Z, Zhao H, Gao F, Wen J, Zhao L, Gui Y, *et al.* Sirt1 regulates acrosome biogenesis by modulating autophagic flux during spermiogenesis in mice. *Development* 2017; 144:441–451.
- Sidjanin DJ, Park AK, Ronchetti A, Martins J, Jackson WT. TBC1D20 mediates autophagy as a key regulator of autophagosome maturation. *Autophagy* 2016; 12:1759–1775.
- 51. Tu C, Li H, Liu X, Wang Y, Li W, Meng L, Wang W, Li Y, Li D, Du J, Lu G, Lin G, *et al.* TDRD7 participates in lens development and spermiogenesis by mediating autophagosome maturation. *Autophagy* 2021; 17:3848–3864.
- Otani H, Tanaka O, Kasai K, Yoshioka T. Development of mitochondrial helical sheath in the middle piece of the mouse spermatid tail: regular dispositions and synchronized changes. *Anat Rec* 1988; 222:26–33.
- 53. Tanaka Y, Kanai Y, Okada Y, Nonaka S, Takeda S, Harada A, Hirokawa N. Targeted disruption of mouse conventional kinesin heavy chain, kif5B, results in abnormal perinuclear clustering of mitochondria. Cell 1998; 93:1147–1158.
- 54. Zhang Y, Ou Y, Cheng M, Saadi HS, Thundathil JC, van der Hoorn FA. KLC3 is involved in sperm tail midpiece formation and sperm function. *Dev Biol* 2012; 366:101–110.
- Choi SY, Huang P, Jenkins GM, Chan DC, Schiller J, Frohman MA. A common lipid links Mfn-mediated mitochondrial fusion and SNARE-regulated exocytosis. Nat Cell Biol 2006; 8: 1255–1262.
- Chen Y, Liang P, Huang Y, Li M, Zhang X, Ding C, Feng J, Zhang Z, Zhang X, Gao Y, Zhang Q, Cao S, et al. Glycerol kinase-like proteins cooperate with Pld6 in regulating sperm mitochondrial sheath formation and male fertility. Cell Discov 2017; 3: 17030.
- Mi Y, Shi Z, Li J. Spata19 is critical for sperm mitochondrial function and male fertility. Mol Reprod Dev 2015; 82:907–913.
- Gaitskell-Phillips G, Martín-Cano FE, da Silva-Álvarez E, Tapia JA,
 Silva A, Gil MC, Ortega-Ferrusola C, Peña FJ. Phosphoproteomics

- for the identification of new mechanisms of cryodamage: the role of SPATA18 in the control of stallion sperm function†. *Biol Reprod* 2023; 108:324–337.
- Fujiki Y, Yoshimoto K, Ohsumi Y. An Arabidopsis homolog of yeast ATG6/VPS30 is essential for pollen germination. *Plant Physiol* 2007; 143:1132–1139.
- Ciechomska IA, Goemans GC, Skepper JN, Tolkovsky AM. Bcl-2 complexed with Beclin-1 maintains full anti-apoptotic function. Oncogene 2009; 28:2128–2141.
- 61. Sanjuan MA, Dillon CP, Tait SW, Moshiach S, Dorsey F, Connell S, Komatsu M, Tanaka K, Cleveland JL, Withoff S, Green DR. Toll-like receptor signalling in macrophages links the autophagy pathway to phagocytosis. *Nature* 2007; 450:1253–1257.
- 62. Ravikumar B, Moreau K, Jahreiss L, Puri C, Rubinsztein DC. Plasma membrane contributes to the formation of pre-autophagosomal structures. *Nat Cell Biol* 2010; **12**:747–757.
- 63. Thoresen SB, Pedersen NM, Liestol K, Stenmark H. A phosphatidylinositol 3-kinase class III sub-complex containing VPS15, VPS34, Beclin 1, UVRAG and BIF-1 regulates cytokinesis and degradative endocytic traffic. Exp Cell Res 2010; 316: 3368–3378.
- 64. Sagona AP, Nezis IP, Pedersen NM, Liestol K, Poulton J, Rusten TE, Skotheim RI, Raiborg C, Stenmark H. PtdIns(3)P controls cytokinesis through KIF13A-mediated recruitment of FYVE-CENT to the midbody. *Nat Cell Biol* 2010; 12: 362–371.